Study on the Impact of Nonlinearity and Noise on the Performance of High-Capacity Broadband Hybrid Raman-EDFA Amplified System

Lidia Galdino, *Member, IEEE, Member, OSA,* Daniel Semrau, *Student Member, IEEE,* Maria Ionescu, *Member, IEEE,* Adrian Edwards, Wayne Pelouch, Steve Desbruslais, Jeanne James, Eric Sillekens, Domaniç Lavery, *Member, IEEE,* Stuart Barnes, Robert I. Killey, *Senior Member, IEEE,* and Polina Bayvel, *Fellow, IEEE, Fellow, OSA*

***Abstract*—We experimentally demonstrated the transmission of 312×35 GBd DP-256QAM over 9×70 km spans using hybrid distributed Raman-EDFA (HRE) amplifiers with a continuous 91 nm gain bandwidth. A total throughput of 120 Tbit/s over 630 km is demonstrated, with a net achievable information rate after SD-FEC of 10.99 bit/symbol. An extensive, theoretical investigation of the noise contributions originating from amplifier, transceiver sub-system and fiber nonlinearity were carried out using the Gaussian noise model in the presence of inter-channel stimulated Raman scattering (ISRS GN model). The ISRS GN model accounts for arbitrary, wavelength dependent signal power profiles along fiber spans, which is vital for the modeling of ultra-wideband transmission, particularly for hybrid Raman-amplified links. The analysis serves to quantify the relative noise contributions and explain the performance achieved. It was found that, due to the low noise HRE amplifier and a transmission distance of 630 km, the noise originating from the transceiver sub-system imposed a penalty of 6 dB in SNR. For this system, the transceiver noise is, therefore, the main limitation to the system throughput.**

***Index Terms*—Hybrid Raman-EDFA amplifier, broadband transmission system, high order modulation format, adaptive rate LDPC decoder.**

I. Introduction

CURRENTLY, fundamental limits on the performance of optical communication systems are imposed by a combination of noise from the transceiver sub-system, the optical amplifiers, as well as signal distortion due to fiber nonlinearity. Advances in digital signal processing (DSP), higher-order modulation formats, coded modulation, high speed electronics, transmission fibers, and broadband optical amplification have resulted in a significant increase in single-mode fiber (SMF)-based system capacity. Recent years have seen several landmark transmission results using SMF [1]–[10], with demonstrations achieving throughputs exceeding 70 Tbit/s over 7,600 km [1] and 50 Tbit/s over 17,107 km [2]. These trans-Atlantic and trans-Pacific records have been enabled by the combination of coded modulation with hybrid probabilistic and geometrical constellation shaping, multi-stage nonlinearity compensation including digital back-propagation, fast least mean square (LMS) equalization and channel-adaptive coding rates. Despite the advantages of low noise hybrid distributed Raman-EDFA amplifiers (HRE), as demonstrated in [3], most of these record throughput demonstrations over trans-Atlantic and trans-Pacific distance were achieved using C+L band EDFA. On the other hand, the record throughput in short, metropolitan transmission distance systems, has been achieved mainly by using amplification techniques operating beyond the operation bandwidth of C+L band EDFAs. In [4], a continuous-band 100 nm semiconductor optical amplifier (SOA) enabled a potential SMF capacity of 115.9 Tbit/s over 100 km. Although the bandwidth is notable, SOAs have a relatively high noise figure compared with distributed Raman amplifiers, so the system performance decreases rapidly with distance. High data throughput in [5] [6] and [7] was achieved by using continuous 90 nm hybrid distributed Raman-EDFA amplifier with data throughput of 120 Tbit/s over 630 km demonstrated in [7] and an overall record throughput of 150.3 Tbit/s over 40 km span [8], achieved by transmitting the signals in the S, C and L-bands.

Despite these impressive advances, a theoretical assessment of the major noise contributions in ultra-wideband, high-capacity transmission has not been investigated on a per-channel basis. This theoretical analysis is important to help identify potential performance bottlenecks and over-engineered sub-systems.

This paper[1] presents a comprehensive analysis of the penalty introduced by the major noise sources arising from the amplifier and transceiver sub-systems, as well as from fiber nonlinearity. The nonlinear interference (NLI) is evaluated using the recently proposed Gaussian noise (GN) model in the

This work was supported by UK EPSRC Program Grant TRANSNET EP/R035342/1 and the Royal Academy of Engineering under the Research Fellowships programme.

L. Galdino, D. Semrau, E. Sillekens, D. Lavery, R. I. Killey and P. Bayvel are with the Optical Networks Group, Department of Electronic and Electrical Engineering, UCL, Torrington Place, London WC1E 7JE, UK. e-mail: (l.galdino@ucl.ac.uk, daniel.semrau.15@ucl.ac.uk, e.sillekens@ucl.ac.uk, d.lavery@ucl.ac.uk, r.killey@ucl.ac.uk and p.bayvel@ucl.ac.uk).

M. Ionescu, A. Edwards, W. Pelouch, and S. Barnes, are with Xtera, Bates House, Church Road, Harold Wood, Essex, UK. e-mail: (maria.ionescu@xtera.com, adrian.edwards@xtera.com, wayne.pelouch@xtera.com, and stuart.barnes@xtera.com).

S. Desbruslais, was with Xtera and now he is with Consultant at Steve Desbreslais Technical Services. email: stephen@desbruslais.plus.com

J. James, was with Xtera. email: jeanne_sabie@hotmail.com

Manuscript received xxx; revised xx, 2017.

[1]This manuscript is an extension of the work presented at the 2018 European Conference on Optical Communications [7].

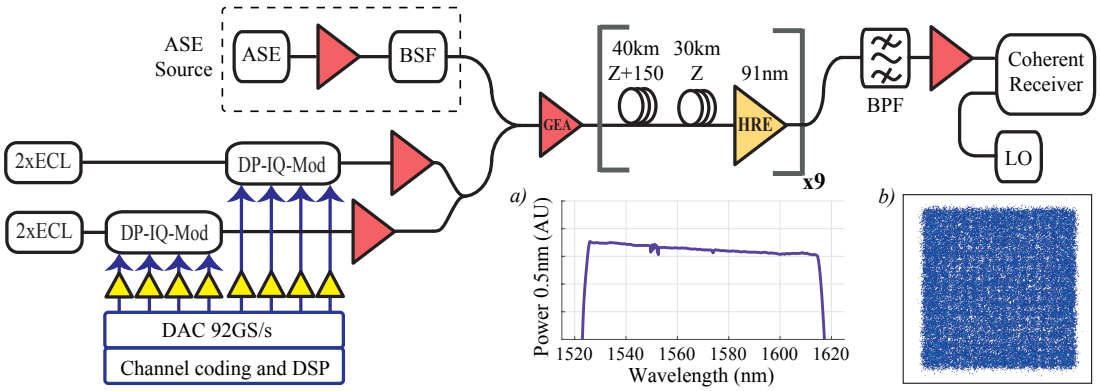

Fig. 1. Experimental configuration; the four channels generated are co-propagated with ASE noise to emulate transmission over the amplifiers' 91 nm gain bandwidth. (a) The transmitted optical spectrum, and (b) the back-to-back measurement of a 256QAM constellation at 1550 nm.

presence of inter-channel stimulated Raman scattering (ISRS) [11]. The model, termed the ISRS GN model, accurately estimates the NLI in ultra-wideband transmission, in which each WDM channel experiences a different effective attenuation. This variation in effective attenuation across the entire transmission bandwidth is a consequence of the varying fiber attenuation, ISRS and the used HRE amplification scheme. The modeling predictions are compared to the experimental findings in terms of signal-to-noise ratio (SNR).

The experimental transmission system under investigation is a 312×35 GBd dual polarization 256-*ary* quadrature amplitude modulation (DP-256QAM) wavelength division multiplexed (WDM) channels over 9×70 km single mode fiber spans. The high channel count is enabled by hybrid distributed Raman-EDFA (HRE) amplifiers with a continuous gain bandwidth of 91 nm. A record throughput over a continuous transmission bandwidth of 120 Tbit/s over a transmission distance of 630 km is reported, with a net information rate of 10.99 bit/symbol after SD-FEC.

The paper is organized as follows. In Section II, the experimental configuration is described. Section III presents the modeling approach and the evaluation of the individual noise components. The experimental and theoretical investigation of the transmission system performance is presented in Section IV, the data throughput estimation using the generalised mutual information and the proposed FEC scheme are described in Section V and the conclusions are in Section VII.

II. Transmission Configuration

The experimental configuration used in this work is shown in Fig. 1. Four carriers, spaced at 35.5 GHz, were connected to two independent dual-polarization IQ optical modulators, each driven by four 92 GS/s digital-to-analogue converters (DACs) to generate four odd/even channels. A digital root-raised cosine (RRC) filter with a 0.01 roll-off was used to spectrally shape the signals and digital pre-emphasis was applied to overcome the electrical response of the transmitter components. The channels were generated at carrier frequencies which were tuned across the range 185.5405 to 196.5810 THz, allowing the measurement of 312×35 GBd DP-256QAM channels, covering the spectrum from 1524.9 to 1615.9 nm.[2]

The modulated channels were amplified using a pair of 97 nm bandwidth discrete Raman amplifiers with 12.5 dB gain and combined with wideband amplified spontaneous emission (ASE) noise, which emulated co-propagating channels over the entire transmitted bandwidth. The ASE noise source, with continuity across the entire 97 nm bandwidth, was generated by a pair of discrete Raman amplifiers, were the output of the first Raman amplifier, illustrated by the ASE box in Fig. 1, is connected to the second Raman amplifier and, followed by a band stop filter (BSF), used to create a notch in the ASE within which the modulated channels were positioned. The validity of using ASE noise to emulate aggressor channels was verified in [12] [13], showing that this technique provides a conservative measure of system performance. This technique has also been used in [4], [14] and [15] to emulate interference channels and estimate transmission system capacity.

A gain equalizing amplifier (GEA) with a continuous 91.04 nm bandwidth was used to amplify and spectrally shape (SS) the combined ASE and modulated channels. The combined SS-ASE and modulated channels occupied a total useable bandwidth of 11.0758 THz (91.04 nm) with a total output power of 22 dBm. The optical spectrum after the GEA is shown as inset (a) in Fig. 1. A power tilt of -2 dB across the bandwidth was applied to optimize channel performance, taking into account the wavelength-dependent noise figure of the transmission line amplifiers. The back-to-back 256QAM constellation is illustrated in the inset (b) of Fig. 1.

The transmission link is comprised of a straight-line link of 9 spans, with 70 km of single-mode fiber and a hybrid distributed Raman-EDFA amplifier (HRE) in each span. Fig. 2 illustrates the schematic of the HRE amplifier. It provides a continuous gain from 1524.9 nm to 1615.9 nm and used two counter-propagating pumps at 1427 and 1495 nm with output powers of 300 mW and 310 mW into the transmission fibre,

[2]Two different types of lasers were used in this experiment: C and L-band external cavity laser (ECL) with 15.5 dBm output power and 100 kHz linewidth was used for the channels wavelength between 1534 - 1566 nm and 1569 - 1610 nm. For the channel wavelengths between 1525 - 1534 nm; 1566 - 1569 nm; and 1610 - 1615 nm, a tunable laser assembly (iTLA) with 13 dBm output power and 200 kHz linewidth was used.

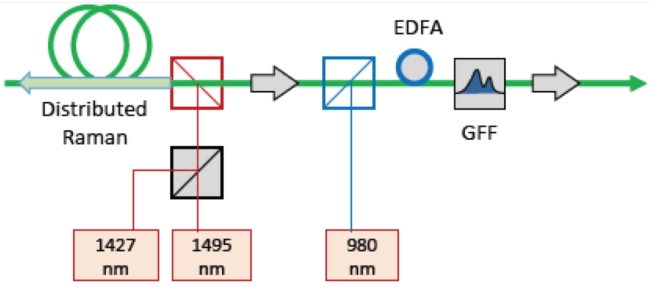

Fig. 2. Schematic of the hybrid Raman EDFA amplifier (HRE).

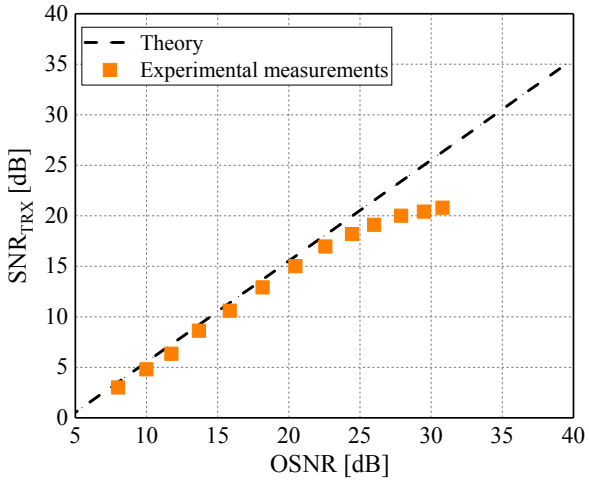

Fig. 3. Back-to-Back measurements of received SNR as a function of OSNR 0.1 nm for a 35 GBd DP-256QAM located at 1550 nm.

delivering a total signal power of 19.5 dBm to the EDFA stage. The single stage EDFA followed by a 91 nm gain flattening filter (GFF), designed to equalize the gain across the entire HRE bandwidth, boosted the signal to a total output power of 22 dBm. Each 70 km fiber span is comprised of two fiber types; the first part of the hybrid span used 40 km of Sumitomo Z+150 fiber with an average attenuation of 0.148 dB/km and an effective core area of 149 μm^2. The second part of the span used 30 km of Sumitomo Z fiber with an average attenuation of 0.16 dB/km and an effective core area 81 μm^2. The second segment of the hybrid span used a lower effective area to increase the Raman gain in the second part of the span for a given pump power.

At the receiver, a bandpass filter (BPF) with a 40 GHz bandwidth was used to filter the channel under test. The transmitter BSF and the receiver BPF were moved together in order to create a notch for the channel under test (channel 2 in the 4-channel group were used for performance measurement), as well as exclude the out-of-band noise from the receiver. The coherent detection was carried out using a phase- and polarization-diverse coherent receiver incorporating 70 GHz bandwidth photodetectors, and the signal was digitized using a real-time oscilloscope with 63 GHz bandwidth, sampling at 160 GSa/s. Digital signal processing was performed as described in [12], which included matched filtering, single step chromatic dispersion compensation, a 21-tap blind adaptive equalizer, frequency offset compensation and decision directed carrier phase estimation.

III. Analytical Model

In order to maximize the amount of data that can be reliably transmitted through a broadband optical communication system, it is crucial to evaluate and maximize the performance of each individual WDM channel. In this work, the major noise contributions governing the system performance, were investigated and quantified, namely the amplifier noise, transceiver noise and nonlinear interference noise.

After coherent detection and electronic dispersion compensation of the i^{th} channel, the channel dependent SNR (herein $\text{SNR}_{\text{Total}_i}$) is comprised of statistically independent noise and distortion components that can be calculated as

$$\frac{1}{\text{SNR}_{\text{Total}_i}} = \frac{1}{\text{SNR}_{\text{TRX}_i}} + \frac{1}{\text{SNR}_{\text{Link}_i}}, \tag{1}$$

and

$$\frac{1}{\text{SNR}_{\text{Link}_i}} = \frac{1}{\text{SNR}_{\text{ASE}_i}} + \frac{1}{\text{SNR}_{\text{NLI}_i}}, \tag{2}$$

where $\text{SNR}_{\text{ASE}_i}$ is the SNR imposed by the amplifier, $\text{SNR}_{\text{NLI}_i}$ is the SNR imposed by the optical fiber and $\text{SNR}_{\text{TRX}_i}$ is the transceiver-constrained SNR (i.e. the back-to-back SNR). This transceiver noise sets an upper limit on the available SNR, and therefore each channel's greatest achievable information rate. This variable includes all phenomenological impairments of the system under test, and it can be accurately measured experimentally, in a back-to-back configuration.

The $\text{SNR}_{\text{ASE}_i}$ is a linear noise source generated by optical amplifiers used in the transmission line to compensate for fiber loss. It accounts for the amplified spontaneous emission (ASE) noise within the bandwidth of the channel, i, and can be calculated as

$$\text{SNR}_{\text{ASE}_i} = \frac{P_i}{N P_{\text{ASE}_i}}, \tag{3}$$

where P_i is the signal launch power N is the number of amplifiers, and P_{ASE} is the ASE noise power within the channel bandwidth. The ASE noise power in a multi-span system can be calculated as $\text{P}_{\text{ASE}_i} \approx G_i \text{NF}_i h \nu_i$, where G_i is the channel-dependent gain (see Fig. 5), NF_i is the noise figure, h is the Planck's constant and ν_i is the channel center frequency.

Finally, as described in detail in [16] $\text{SNR}_{\text{NLI}_i}$ accounts for nonlinear noise arising from fiber nonlinearity and it can be written as

$$\text{SNR}_{\text{NLI}i} = \frac{P_i}{P_{\text{NLI}_i}} = \frac{P_i}{N^{1+\epsilon_i} \eta_i P_i^3}, \tag{4}$$

where ϵ_i is the coherence factor and η_i is the nonlinear interference coefficent of channel i. It should be noted that for ultra-wideband transmission, where ISRS is significant, the NLI coeffcient η_i is a function of the total input launch power and its spectral distribution [16], [17], [22].

The total SNR ($\text{SNR}_{\text{Total}i}$) can be expressed as [16]

$$\text{SNR}_{\text{Total}i} = \frac{P_i}{\kappa P_i + N P_{\text{ASE}_i} + N^{1+\epsilon_i} \eta_i P_i^3}, \tag{5}$$

where $\kappa = 1/\text{SNR}_{\text{TRX}}$.

IV. Results

In order to understand the impact of each noise source contribution on the $\text{SNR}_{\text{Total}_i}$, and therefore, its impact on the overall data throughput of the transmission system under test, in this section each noise source contribution is individually assessed.

A. Transceiver Noise

To investigate the transceiver noise contribution, in this subsection, the back-to-back performance of the system under test is quantified. The back-to-back signal-to-noise ratio ($\text{SNR}_{\text{TRX}_i}$) versus OSNR, over both polarisation, with channel i located at 1550 nm is shown in Fig. 3.

The experimentally measured $\text{SNR}_{\text{TRX}_i}$ was recorded by connecting the output of the GEA amplifier straight to the BPF filter (see Fig. 1) and ASE was added to the signal to vary the OSNR. The same equaliser filter, that generated the channel power tilt across the 91 nm bandwidth, was used for back-to-back SNR_{TRX} measurements. Therefore its impairments contributed to the back-to-back implementation penalty. The $\text{SNR}_{\text{TRX}_i}$ was evaluated as the ratio between the variance of the transmitted symbols $E[|X|^2]$ and the variance of the noise σ^2, where $\sigma^2 = E[|X - Y|^2]$ and Y represents the received symbols after DSP is applied. The theoretical calculation of OSNR in 0.1 nm bandwidth is given by $\text{OSNR} = \text{SNR}_{\text{TRX}_i} + 10\log_{10}(\text{R}_\text{s}/\text{B})$, where R_s is the symbol rate and B is the noise bandwidth, is also shown to provide a performance reference relative to the experimental results. It can be seen that the highest measured SNR_{TRX} and OSNR on this back-to-back subsystem was 20.8 dB and 31 dB, respectively. It can also be noted that at lower OSNR regime, where the system is mainly limited by ASE noise, a penalty in experimentally measured SNR, compared with the theoretical limit, was observed. This is still due the noise contribution of the transceiver constrained SNR_{TRX}. A detail analysis of transmitter and receiver noise contribution can be found in [18]. The SNR_{TRX} noise source contribution is mainly due to the low effective number of bits (ENOB) from digital to analog converters (DACs) and analog to digital converters (ADCs)and noise figure from the linear amplifiers to drive the modulators. [18] [19] [20]. The DACs and ADCs in the real time sampling oscilloscope exhibited a frequency dependent ENOB, of 5 and 4.8 bits at a frequency of 15 GHz, respectively. The linear amplifiers to drive the modulator, each have a noise figure of 6 dB.

Aside from the electrical noise from the transceiver subsystem, the highest achievable SNR_{TRX} is further limited by non-ideal digital signal processing (DSP) and ASE noise introduced by optical amplifiers needed to compensate for optical losses on the back-to-back experimental setup, including those from the modulators (insertion + modulation loss, typically 24 dB). In this case of continuous broadband system [20], which required high noise figure continuous lumped Raman amplifier to compensated for optical losses on the back-to-back setup, the highest measured OSNR was only 31 dB, before the signals is launched into the transmission fiber. A way to enhance this OSNR is to place an optical amplifier before the modulator, however for broadband continuous transmission systems, with bandwidths beyond C+L band EDFAs, this is challenging as any other lumped optical amplifier technology is based on nonlinear devices, such as lumped Raman

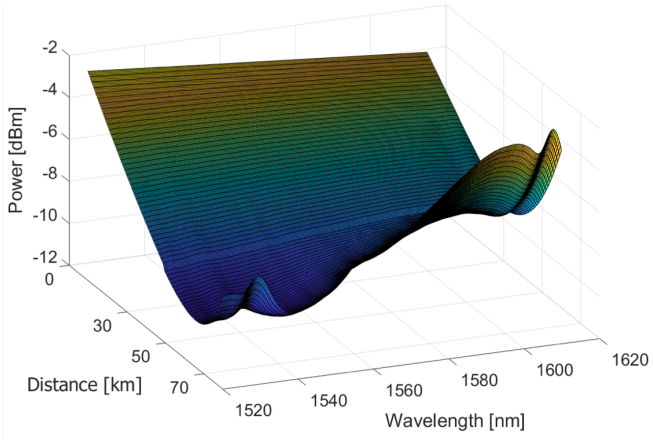

Fig. 4. Signal power profile over one span obtained by numerically solving the Raman equations. An average channel launch power of -3.5dBm with a slop of -0.014dBm with was considered.

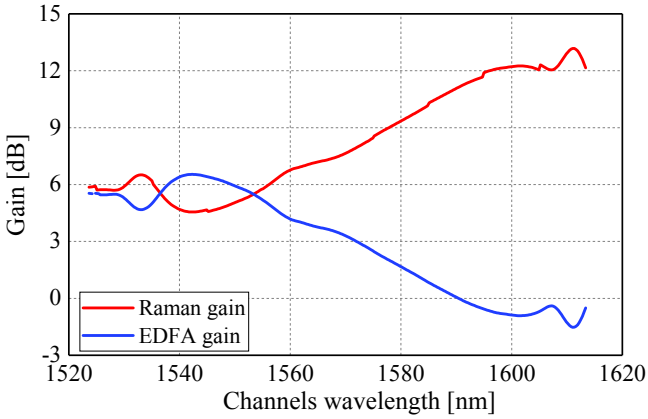

Fig. 5. Gain for the distributed Raman and EDFA amplification stage. The gain of the distributed Raman amplification stage is the accumulated gain over one span.

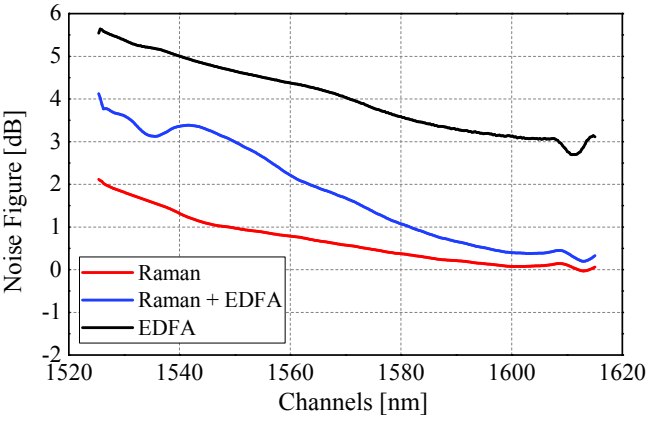

Fig. 6. Effective noise figure of the hybrid Raman-EDFA amplifier that was used to compensate for the span loss.

or semiconductor optical amplifier (SOA), which generate nonlinear effects such as four wave mixing and stimulated Brillouin scattering. These are specific challenges in design of a state-of-the-art, advanced and flexible experimental platform - commercial systems would, of course, have independent transceivers. The $\mathrm{SNR_{TRX}}$ back-to-back measurements was taken for few wavelengths across the entire 91 nm bandwidth, and expected, a very similar performance was found. Therefore, for the system modeling a $\mathrm{SNR_{TRX_i}}$ of 20.8 dB was considered for all i channels.

B. Amplifier Noise

In this subsection, the linear noise power contribution of the HRE amplifier limiting the system performance is investigated. The first step to estimate the linear noise power is to simulate the signal power profile across the entire 91 nm of bandwidth as illustrated in Fig. 4. The frequency dependent signal power profile can be obtained by solving a set of coupled ordinary differential equations [21]

$$\begin{aligned}
\frac{\partial P_i}{\partial z} =& -\underbrace{\sum_{k=i+1}^{M}\frac{f_i}{f_k}g_{\mathrm{r}}(\Delta f)P_kP_i}_{\text{ISRS loss}}+\underbrace{\sum_{k=1}^{i-1}g_{\mathrm{r}}(\Delta f)P_kP_i}_{\text{ISRS gain}}\\
&+\underbrace{\sum_{k=1}^{2}g_{\mathrm{r}}(\Delta f)P_{\mathrm{p},k}P_i}_{\text{distributed amplification}}-\alpha\left(f_i\right)P_i,\\
\frac{\partial P_{\mathrm{p},1}}{\partial z} =& +\underbrace{\sum_{k=1}^{M}\frac{f_{\mathrm{p},1}}{f_k}g_{\mathrm{r}}(\Delta f)P_kP_{\mathrm{p},1}}_{\text{signal pump depletion}}-\underbrace{g_{\mathrm{r}}(\Delta f)P_{\mathrm{p},2}P_{\mathrm{p},1}}_{\text{distributed amplification}}\\
&+\alpha\left(f_{\mathrm{p},1}\right)P_{\mathrm{p},1},\\
\frac{\partial P_{\mathrm{p},2}}{\partial z} =& +\underbrace{\sum_{k=1}^{M}\frac{f_{\mathrm{p},2}}{f_k}g_{\mathrm{r}}(\Delta f)P_kP_{\mathrm{p},2}}_{\text{signal pump depletion}}+\underbrace{\frac{f_{\mathrm{p},2}}{f_{\mathrm{p},1}}g_{\mathrm{r}}(\Delta f)P_{\mathrm{p},1}P_{\mathrm{p},2}}_{\text{pump pump depletion}}\\
&+\alpha\left(f_{\mathrm{p},2}\right)P_{\mathrm{p},2},
\end{aligned} \tag{6}$$

where P_i, f_i are the power and center frequency of signal channel i, $P_{\mathrm{p},k}$, $f_{\mathrm{p},k}$ are the power and center frequency of pump k, M is the total number of WDM channels, $g_r(\Delta f)$ is the polarization averaged, normalized (by the effective core area A_{eff}) Raman gain spectrum for a frequency separation Δf of the interacting channels and $\alpha\left(f\right)$ is the frequency dependent attenuation coefficient. Eq. (6) is indexed such that P_1 is the signal channel with the highest center frequency and $z = 0$ references the beginning of the fiber span. The normalized power profile for a particular channel center frequency f_i is defined as $\rho\left(z, f_i\right) = \frac{P_i(z)}{P_i(0)}$. The continuous interpolation of all signal channels $\rho\left(z, f_i\right)$ yields the signal power profile for a generic frequency component $\rho\left(z, f\right)$.

Eq. (6) takes into account the Raman pumps at 1427 and 1495 nm with 300 mW and 310 mW, respectively, wavelength-dependent fiber attenuation, inter-channel Raman scattering, pump depletion, transmission fiber parameters as described on Section II, and an average channel launch power of -3.5 dBm with average channel launch power of -3.5 dBm with a slope of -0.014 dB/nm ,which was deemed to be optimal. Note that, due to implementation constrains, a power tilt of 2 dB was considered on the experimental setup.

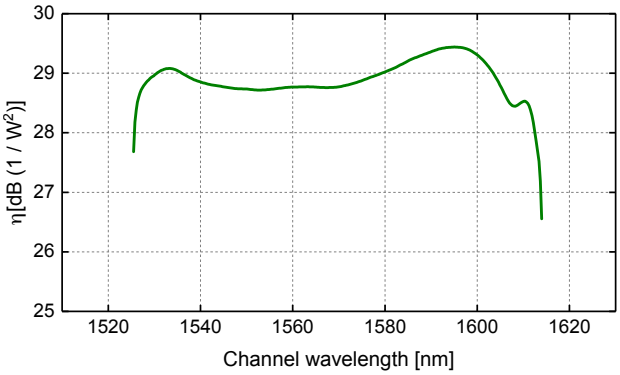

Fig. 7. NLI after one spans as a function of wavelength obtained by numerically integrating the ISRS GN model with a signal power profile as shown in Fig. 4

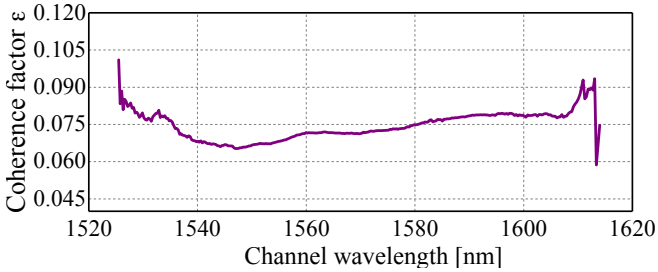

Fig. 8. Coherence factor as a function of channel wavelength obtained by numerically integrating the ISRS GN model.

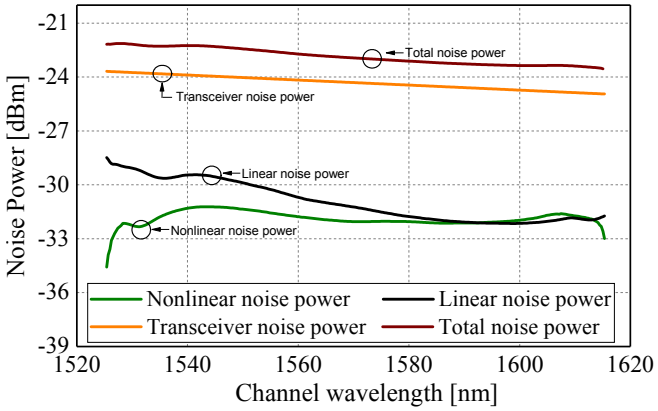

Fig. 9. Noise power for the major noise components as a function of channel wavelength after 630 km transmission.

The distributed Raman gain can than be obtained from the signal power profile, as shown in Fig. 4. The EDFA gain was than set to recover the input power distribution, and it is illustrated in Fig. 5. In order to estimate the ASE noise power it is also crucial to know the the frequency-dependent noise figure (NF) of the HRE amplifier. Fig. 6 illustrates the NF experimental measurements of the EDFA only (black line), distributed Raman amplifier only (red line) and the total NF (blue line). The distributed amplification approach reduces the NF compared to lumped amplification scheme; reducing the effective NF to only 1.4 dB on average.

C. Nonlinear Interference Noise

The recently proposed ISRS GN model was used to calculate the nonlinear interference coefficient [11], [23], [24]. The ISRS GN model represents an extension of the conventional GN model [25], to account for wavelength dependent signal power profiles along fiber spans. Wavelength dependent signal power profiles arise from varying fiber attenuation, ISRS and distributed Raman amplification. In the context of HRE amplification, the ISRS GN model in semi-analytical form must be used, which is [11, Eq. (4)]

$$\eta_i = \frac{16}{27}\gamma^2 \frac{B_{\text{ch}}}{P_i^3} \int df_1 \int df_2 \; G_{\text{Tx}}(f_1) G_{\text{Tx}}(f_2) G_{\text{Tx}}(f_1+f_2-f) \cdot \left| \int_0^L d\zeta \sqrt{\frac{\rho(\zeta,f_1)\rho(\zeta,f_2)\rho(\zeta,f_1+f_2-f)}{\rho(\zeta,f)}} e^{j\phi(f_1,f_2,f,\zeta)} \right|^2, \tag{7}$$

where $G_{\text{Tx}}(f)$ is the spectral power density at the fber input, B_{ch} is the channel bandwidth, $\phi = -4\pi^2(f_1-f)(f_2-f)\left[\beta_2 + \pi\beta_3(f_1+f_2)\right]\zeta$, β_2 is the group velocity dispersion (GVD) parameter, β_3 is the linear slope of the GVD parameter, γ is the nonlinearity coefficient and $\rho(z,f)$ is the normalized signal power profile. The signal power profile was obtained from numerically solving the Raman equations (6) over the two fiber types and then inserted in the analytical model.

The NLI coefficient after one span as a function of the channel wavelength is illustrated in Fig. 7. The results account for average channel launch power of -3.5 dBm with a slope of -0.014 dB/nm, wavelength dependent dispersion and a wavelength dependent effective core area. The signal power profile, shown in Fig. 4, was used to take into account wavelength dependent attenuation, ISRS, distributed Raman amplification, pump depletion and coupling losses between the two fiber types, as specified in Section II. The modulation format dependence was corrected for the four 256-QAM modulated channels using [26] and assumed a lumped-like power profile. In the modulation format correction it is assumed that ISRS does not significantly alter the *relative* modulation format dependence, which is supported by the results in [23].

The coherence factor ϵ is illustrated in Fig. 8. It was obtained using numerically integrating the ISRS GN model for multiple spans, where the signal power profile is extended for multiple spans n by $\rho\,(z+L) = \rho\,(z)$. Different launch power distributions launched into different spans can be accounted for by solving (6) for *each* span separately in order to yield the signal power profile for the entire link and normalizing by the launch power at the transmitter. The irregular fluctuations in the coherence factor, as depict in Fig. 8, are a consequence of the numerical integration.

D. System noise Sources and their relative contributions

In this subsection, the contribution of each noise source to limiting the received $\text{SNR}_{\text{Total}_i}$ of each channel after 630 km (9 x 70 km) is investigated. Fig. 9 illustrates the noise power of each noise and distortion components after 630 km as a function of channel wavelength. The black line shows the linear noise power P_{ASE_i} generated by the HRE amplifier, the green line depicts the nonlinear noise power P_{NLI_i} related to the fiber span, the orange line illustrates the transceiver noise power $P_{\text{TRX}} = \kappa P_i$, given by the transceiver subsystem constrained-SNR, and the brown line shows the total noise power $\text{P}_{\text{Total}_i}$ for each channel, which is given by the sum of this three noise source. It is clear that the predominant noise power in this transmission system is given by the transceiver subsystem, with a mean P_{TRX} of -24.3 dBm, while the mean total noise power P_{Total} was estimated to be -22.8 dBm.

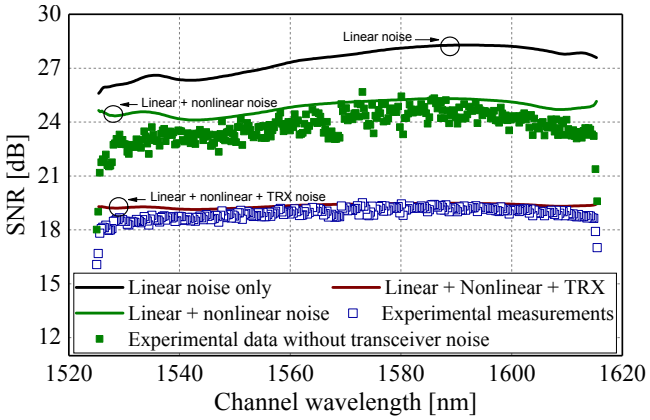

Fig. 10. Signal-to-noise ratio including different noise components as a function of channel wavelength after 630 km transmission.

To quantify the impact of each noise source contribution to the received $\text{SNR}_{\text{Total}_i}$ of each channel, Fig. 10 shows the variation of SNR after 630 km with channel wavelength. The black line is the SNR calculated assuming the presence of linear noise power only, the green line shows the $\text{SNR}_{\text{Link}_i}$, which takes into account the linear noise power of the in line HRE amplifier and nonlinear noise power from the optical fiber. The brown line shows the received $\text{SNR}_{\text{Total}_i}$ taking into account all noise contributions (linear, nonlinear and transceiver). The square blue markers illustrates the experimentally measured $\text{SNR}_{\text{Total}_i}$ after 630 km. A penalty in the mean SNR due to nonlinear interference noise was found to be only 2.6 dB, providing a mean link SNR of 24.8 dB. By adding the transceiver noise, the received SNR further decreases to 19.8 dB; a 5 dB penalty on the $\text{SNR}_{\text{Total}}$ due to the transceiver noise only. The $\text{SNR}_{\text{Total}}$ experimentally measured shows a very good agreement with the $\text{SNR}_{\text{Total}}$ modeling prediction. We also compare the SNR_{Link} noise contribution from experimental data within the modelling results (green line). The green makers in Fig. 10 depict the SNR_{Link} of the experimental data, which was estimated by extracting the transceiver noise component. By rearranging Eq. (1), such as, $1/\text{SNR}_{\text{Link}_i} = 1/\text{SNR}_{\text{Total}_i} - 1/\text{SNR}_{\text{TRX}}$ is possible to extract the SNR_{TRX} from the experimental measurements. The mean SNR_{Link} predicted by the model is 24.8 dB, while the mean SNR_{Link} of the experimental data was found to be 23.8 dB; 1 dB difference between modelling prediction and experimental data.

This discrepancy between experimental results and modelling prediction may be due to experiments inaccuracies and uncertainties, i.e. the model assumes that all in line amplifiers

generates exactly the same amount of noise power; doesn't consider extra losses due to fiber splicing and connection between the spans; the two different types of lasers used to across the entire bandwidth (see footnote 2), which are likely to be the cause of worse performance at lower and high wavelengths compared to the central wavelengths. In addition to potential mismatches between experimental and theoretical parameters, inaccuracies may stem from intrinsic model assumptions. Such assumptions include the validity of the first-order perturbation approach, negligible temporal gain dynamics of ISRS and negligible impact of polarization mode dispersion on the Kerr nonlinearity.

Nevertheless, the aim of this set of result was to explain these experimental results with the help of modelling to identify the contribution of each noise source to the transmission system. As a consequence of this analysis, it showed that the transceiver noise is the predominant noise contribution in the system under investigation.

V. Data Throughput

The generalised mutual information (GMI), a metric that measure the achievable rates of BICM systems with bit-metric mismatched decoding was used to quantify the achievable rate of each individual channel. The GMI estimation was based on unscaled LLRs calculated for the AWGN auxiliary channel [29, Eq. (30)].

For channel decoding, the proposed FEC scheme is a concatenation of an outer hard decision Bose-Chaudhuri-Hocquenghem code (BCH) [27] and an inner irregular repeat accumulate LDPC code (proposed in the DVB-S2 standard [28]) of rate Rc .

To obtain a larger family of code rates, the other LDPC code rates were achieved via pseudorandom puncturing patterns. This configuration was previously proposed and used in [29]. The inner LDPC code was implemented offline in MATLAB. This enabled the FEC overhead to be tailored to each one of the 312 PDM-256QAM channels. The rate of the outer BCH was chosen to be 0.5% overhead [BCH]. This code produces a post-FEC bit error ratio (BER) of 10^{-15} for a post-LDPC BER of 3×10^{-4}. If the post-LDPC BER was below the SCC threshold (3×10^{-4}), a post-FEC BER of 10^{-15} was assumed.

Fig. 11 plots the experimentally measured information rate of all 312 x 35 GBd DP-256QAM channels, including the 0.5 GHz channel gap. The green diamonds show the Shannon limit for the received SNR given by $\log_2(1+\mathrm{SNR}_{\mathrm{Total}_i})$ summed over both polarisations. The blue triangles depict the pre-FEC GMI calculated using received log-likelihood ratios. The post-FEC rate after inner and outer FEC is plotted by the red circles. A mean penalty of 0.94 bit/symbol between the GMI (11.62 bit/symbol) and the Shannon limit (12.56 bit/symbol) is due to the use of non-optimal finite constellation and bit labeling. For the net rate after FEC, the occupied spectrum yields a net bit rate of 10.99 bit/symbol providing a record single mode fibre capacity of 120.0 Tbit/s. The performance at the edge of the transmission bandwidth drops very quickly because the channels are located at the roll-off of the HRE-amplifier bandwidth.

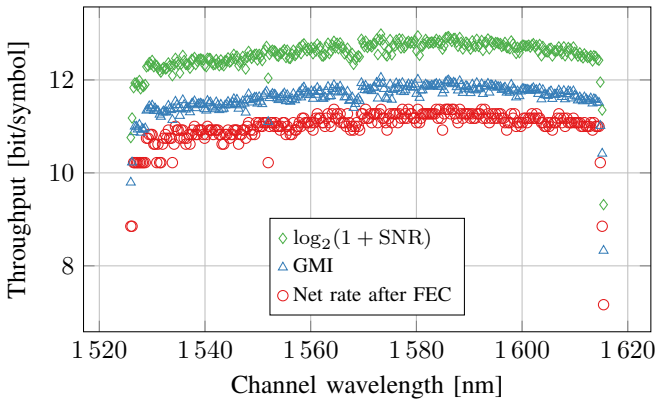

Fig. 11. Throughput per channel over 2 polarizations after a transmission distance of 630 km.

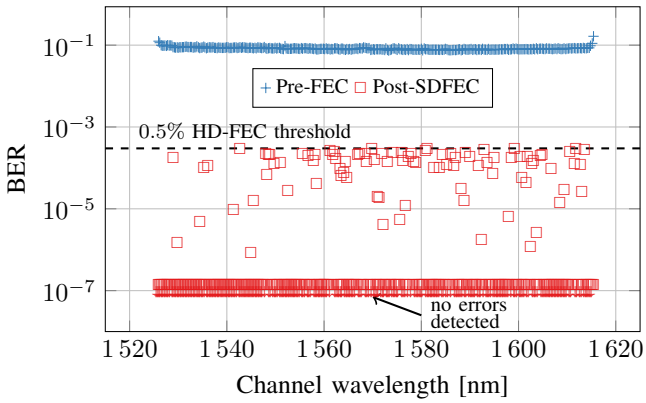

Fig. 12. Pre-FEC and Post-SDFEC bit error rate for all 312 channels. Arrows indicate channels where no errors were observed after post-SDFEC.

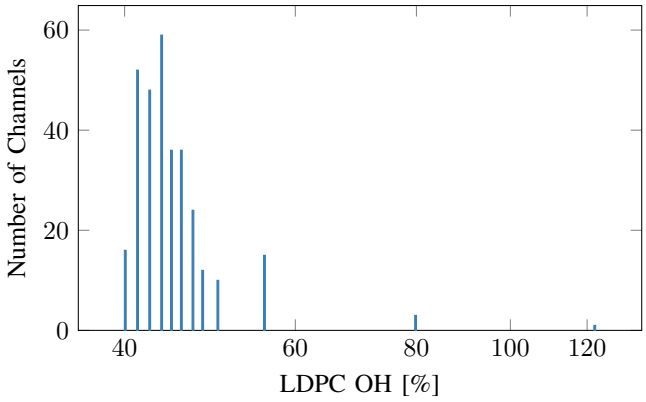

Fig. 13. LDPC overhead usages.

Fig. 12 shows the pre- and post-SDFEC BER for all 312 channels. The channels were decoded using 12 rate adapted LDPC codes implemented from the DVB-S2x. All 312 channels were measured, confirming the total net throughput of 120.0 Tbit/s. Fig. 13 shows the rates used for the SDFEC after which all channels were below the BER threshold for the outer HDFEC. The bulk of the codewords have a low spread, 293 out of 312 are between 40-50% FEC overhead. Reducing the number of 7 code rates applied was found to reduce the total net data throughput to 119.0 Tbit/s.

VI. Impact of Transceiver Subsystem on Overall System Performance

In previous Sections the impact of the transceiver noise was demonstrated for a fixed transmission distance and a given transceiver constrained-SNR. This Section is dedicated to investigating the implications of transceiver noise on the overall system performance for a range of transmission distances. The basic SNR model described in Section III was used to estimate the received SNR. The ISRS GN-model [11] was used to calculate the nonlinear interference noise (NLI) of each channel per span, as shown in Fig. 7, as well as the

HRE amplifier linear noise power per span. Fig. 14, shows the ISRS GN-model prediction of mean received SNR_{Total} of the 312 channels as a function of distance and different transceiver noise contribution. The black line illustrates the model prediction of the mean receiver SNR_{Total} when the transceiver subsystem is ideal ($SNR_{TRX} = \infty$, therefore $SNR_{Total} = SNR_{Link}$). The other lines illustrate the transmission system performance for a range of transceiver noise. As already described in Fig 10, after 630 km the mean received SNR_{Total} with an ideal transceiver is 24.8 dB. When a transceiver noise of 20.8 dB was taken into account, the mean received SNR_{Total} reduced to 19.8 dB; yielding a decrease in received SNR of 5 dB. Additionally, for the particular transmission system under investigation, the transmission distance could have been increased to 1890 km (3 times longer than 630 km) in the absence of transceiver noise.

Furthermore, as illustrated by the blue line, a subsystem with SNR_{TRX} of 25 dB (which is the highest transceiver SNR report to date for a 35 GBd signal using commercial off-the-shelf 92 GS/s DACs with CMOS technology [19]), yield a decrease in the received SNR_{Total} compared to an ideal transceiver of 2.9 dB after 630 km; 1.7 dB after 1260 km; 0.9 dB after 2520 km and only 0.5 dB after a trans-Atlantic distance of 5040 km. This plot also indicates that, for this range of transceiver-limited SNR, up to 1,000 km, the transceiver noise is the predominant noise source on this transmission system under investigation. In ultra-long haul distance the system performance becomes dominated by the amplifier noise and fiber nonlinear noise.

VII. Conclusions

Theoretical modelling together with the results of an experimental investigation were used to characterise the performance of high capacity broadband transmission system, on a per-channel basis. The transmission system under investigation was 312x35 GBd DP-256QAM over 9 x 70 km spans using hybrid distributed Raman-EDFA (HRE) amplifiers with a continuous 91 nm gain bandwidth. A SNR model was used to evaluate the contribution of each individual noise source (transceiver subsystem, line amplifier, and fiber nonlinearity) to the overall transmission system performance. The Gaussian Noise Model in the presence of inter-channel stimulated Raman scattering ISRS GN model was used to predict the nonlinear interference coefficient for each individual channel. It was identified that for this 630km system, the transceiver noise is the main noise source contribution limiting the transmission system throughput. A net data throughput of 120 Tbit/s over 630 km was experimentally demonstrated and a good agreement between the theoretical model and the experimental data was found over the entire 91nm transmission bandwidth.

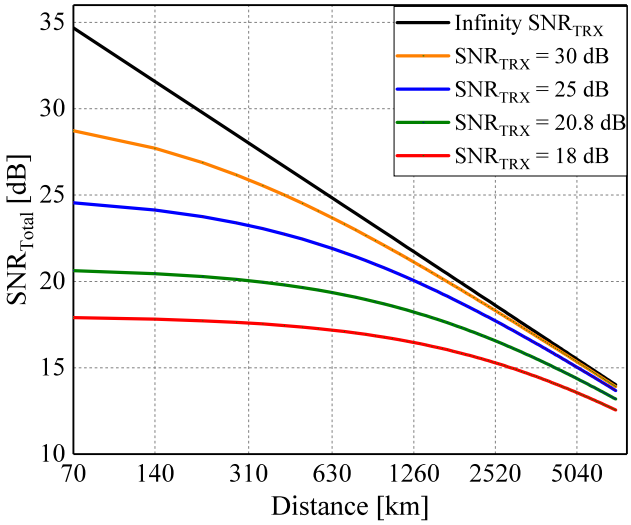

Fig. 14. Total signal-to-noise ratio versus distance for different transceiver noise.

Acknowledgment

The authors wish to thank the Royal Academy of Engineering under the Research Fellowships scheme for Dr Lidia Galdino and Dr Domaniç Lavery. The support from UK EPSRC Program Grant TRANSNET EP/R035342/1 is gratefully acknowledged. The authors are grateful to Sumitomo for their support in this investigation and Oclaro for the use of the high bandwidth, four-dimensional modulators.

References

[1] J.-X. Cai *et al.*, "70.46 Tb/s over 7,600 km in in C+ L Band Using Coded Modulation with Hybrid Constellation Shaping and Nonlinearity Compensation, Proc. OFC, PDP Th5B.2, 2017.

[2] J.-X. Cai *et al.*, "51.5 Tbps Capacity over 17,107 km in C+L Bandwidth Using Single-Mode Fibers and Nonlinearity Compensation, J. Lightw. Technol., vol. 36, no. 11, 2018.

[3] J.-X. Cai *et al.*, "49.3 Tb/s Transmission Over 9100 km Using C+L EDFA and 54 Tb/s Transmission Over 9150 km Using Hybrid-Raman EDFA, J. Lightw. Technol., vol. 33, no. 13, 2015.

[4] J. Renaudier *et al.*, "First 100-nm Continuous-Band WDM Transmission System with 115 Tb/s Transport over 100 km Using Novel Ultra-Wideband Semiconductor Optical Amplifiers," Proc. ECOC, PDP, 2017.

[5] A. Sano *et al.*, "102.3-Tb/s C-band extended L-band all Raman transmission over 240 km using PDM-64QAM single carrier FDM with digital pilot tone," Proc. OFC, PDPSC.3, 2012.

[6] D. Qian *et al.*, "101.7-Tb/s (370x294-Gb/s) PDM-128QAM-OFDM Transmission over 3x55-km SSMF using Pilot-based Phase Noise Mitigation," Proc. OFC, PDPB.5, 2011.

[7] M. Ionescu *et al.*, "90 nm C + L Hybrid Distributed Raman/Erbium-Doped amplifier for High Capacity Subsea Transmission," Proc. ECOC, Mo4G.2, 2018.

[8] F. Hamaoka *et al.*, "150.3-Tb/s Ultra-Wideband (S,C and L bands) Single-MOde Fibre Transmission over 40-km Using¿519GB/s/λ PDM-128QAM Signals," Proc. ECOC, Mo4G.1, 2018.

[9] J.-X. Cai *et al.*, "94.9 Tb/s Singl Mode Capacity Demonstration over 1.900 km with C+L EDFAs and Coded Modulation," Proc. ECOC, Mo4G.3, 2018.

[10] A. Ghazisaeidi *et al.*, "Advanced C+L-Band Transoceanic Transmission Systems Based on Probabilistically Shaped PDM-64QAM, J. Lightw. Technol., vol. 35, no. 7, 2017.
[11] D. Semrau *et al.*, "The Gaussian Noise Mode in the Presence of Inter-Channel Stimulated Raman Scattering," J. Lightw. Technol., vol. 36, no. 14, 2018.
[12] D. J. Elson *et al.*, "Investigation of Bandwidth Loading in Optical Fibre Transmission using Amplified Spontaneous Emission Noise," Optics Express, vol. 25, no. 16, 2017.
[13] J.-X. Cai *et al.*, "On the Effects of Transmitter Induced Channel Correlation in Broadband WDM Transmission," Proc. OFC, Th1C.1, 2018.
[14] R. Ryf *et al.*, "White Gaussian Noise Based Capacity Estimate and Characterization of Fiber-Optic Links," Proc. OFC, W1G.2, 2018.
[15] J. Cho *et al.*, "Trans-atlantic field trial using probabilistically shaped 64-QAM at high spectral efficiencies and single-carrier real-time 250-gb/s 16-QAM," Proc. OFC, PDP Th5B.3, 2017.
[16] D. Semrau *et al.*, "Achievable rate degradation of ultra-wideband coherent fiber communication systems due to stimulated Raman scattering," Optics Express, vol. 25, no. 12, 2017.
[17] G.Saavedra *et al.*, "Inter-channel Stimulated Raman Scattering and its Impact in Wideband Transmission Systems," Proc. OFC, Th1C.3, 2018.
[18] L. Galdino *et al.*, "Impact of Transceiver Subsystem on Digital Back Propagation," Proc. IPC, 2018.
[19] L. Galdino *et al.*, "The trade-off Between Transceiver Capacity and Symbol Rate," Proc. OFC, W1B.4, 2018.
[20] L. Galdino *et al.*, "Impact of Transceiver Subsystems on High-Capacity Optical Transmission," Proc. SPPCom, SpTh2G.1, 2018.
[21] S. Tariq *et al.*, "A computer model of non-dispersion-limited stimulated Raman scattering in optical fiber multiple-channel communi- cations, J. Lightw. Technol., vol. 11, no. 12, 1993.
[22] M. Cantono *et al.*, "Physical Layer Performance of Multi-Band Optical Line Systems Using Raman Amplification, J. of Opt. Communications and Networking Vol. 11, no. 1, 2019.
[23] D. Semrau *et al.*, "The ISRS GN Model, an Efficient Tool in Modeling Ultra-Wideband Transmission in Point-to-Point and Network Scenarios," Proc. ECOC, Tu4G.6, 2018.
[24] D. Semrau *et al.*, "A Closed-Form Approximation of the Gaussian Noise Model in the Presence of Inter-Channel Stimulated Raman Scattering," arXiv-eprints, arxiv:1808.07940v2, 2018.
[25] P. Pioggolini, "The GN Model of Non-Linear Propagation in Uncompensated Coherent Optical Systems, J. Lightw. Technol., vol. 30, no. 24, 2012.
[26] A. Carena *et al.*, "EGN model of non-linear fiber propagation," Optics Express, vol. 22, no. 13, 2014.
[27] W. W. Peterson *et al.*, "Error-correcting codes," 2nd. ed., Cambridge, USA, MIT Press, 1972.
[28] ETSI, "Digital video broadcasting (DVB); Second generation framing structure, channel coding and modulation systems for broadcasting, interactive services, news gathering and other broadband satellite applications (DVB-S2)," ETSI, Tech. Rep. ETSI EN 302 307 V1.2.1, 2009.
[29] A. Alvarado *et al.*, "Replacing the soft FEC limit paradigm in the design of optical communication systems," J. Lightw. Technol., vol. 33, no. 20, 2015.